Fitting a 3D Morphable Model to Edges: A Comparison Between Hard and Soft Correspondences

Anil Bas, William A. P. Smith, Timo Bolkart, Stefanie Wuhrer

FITTING A 3D MORPHABLE MODEL TO EDGES: A COMPARISON BETWEEN HARD AND SOFT CORRESPONDENCES

Anil Bas[⋆] *William A. P. Smith*[⋆] *Timo Bolkart*[†] *Stefanie Wuhrer*[‡]

[⋆] Department of Computer Science, University of York, UK
[†] Multimodal Computing and Interaction, Saarland University, Germany
[‡] Morpheo Team, INRIA Grenoble Rhône-Alpes, France

ABSTRACT

We propose a fully automatic method for fitting a 3D morphable model to single face images in arbitrary pose and lighting. Our approach relies on geometric features (edges and landmarks) and, inspired by the iterated closest point algorithm, is based on computing hard correspondences between model vertices and edge pixels. We demonstrate that this is superior to previous work that uses soft correspondences to form an edge-derived cost surface that is minimised by non-linear optimisation.

***Index Terms*—** 3D morphable model, edge detection, iterated closest point, face shape estimation

1. INTRODUCTION

Image edges convey important information about a face. The occluding boundary provides direct information about 3D shape, for example a profile view reveals strong information about the shape of the nose. Internal edges, caused by texture changes, high curvature or self occlusion, provide information about the position and shape of features such as lips, eyebrows and the nose. This information provides a cue for estimating 3D face shape from 2D images or, more generally, for fitting face models to images.

An early example of using image edges for face model fitting is the Active Shape Model (ASM) [1]. An ASM captures variations in 2D boundary shape. To fit the model to an image, a local search around boundary vertices seeks to align model boundaries with image edges. In 3D, contours extracted from profile views have been used directly for 3D face shape estimation [2] and indirectly as a feature for fitting a 3D morphable model (3DMM) [3]. The earliest work in this direction was due to Moghaddam et al. [4] who fitted a 3DMM to silhouettes extracted from multiple views. From a theoretical standpoint, Lüthi et al. [5] explored to what degree face shape is constrained when contours are fixed.

Romdhani et al. [6] include an edge distance cost as part of a hybrid energy function. Texture and outer (silhouette) contours are used in a similar way to the LM-ICP [7] where correspondence between image edges and model contours is "soft". This is achieved by applying a Euclidean distance transform to the output of an edge detector. This provides a smoothly varying cost surface whose value at a pixel indicates the distance (and its gradient, the direction) to the closest edge. This idea was extended by Amberg et al. [8] who use it in a multi-view setting and improve the robustness of the edge distance cost by integrating over multiple edge detector parameter settings. In this way, the cost surface encodes the saliency of an edge. Keller et al. [9] showed that such approaches lead to a cost function that is neither continuous nor differentiable. This suggests the optimisation method must be carefully chosen. A recent alternative to optimisation-based approaches is to learn a regressor directly from extracted face contours to 3DMM shape parameters [10].

Besides edges, 2D landmarks have long been used [3] as a way to initialize a morphable model fit. Breuer et al. [11] obtained this initialisation using a landmark detector providing a fully automatic system. However, more recently, landmarks have been shown to be sufficient for obtaining useful shape estimates in their own right [12]. Furthermore, noisily detected landmarks can be filtered using a model [13] and automatic landmark detection can be integrated into a fitting algorithm [14]. Instead of landmarks, local features can be used to aid the morphable model fitting [15].

Fitting a 3DMM to a 2D image using only geometric features (i.e. landmarks and edges) is essentially a non-rigid alignment problem. Surprisingly, the idea of employing an iterated closest point [16] approach with hard edge correspondences (in a similar manner to ASM fitting) has been discounted in the literature [6]. In this paper, we pursue this idea and develop an iterative 3DMM fitting algorithm that is fully automatic, simple and efficient (and we make our implementation available[1]). Instead of working in a transformed distance-to-edge space and treating correspondences as "soft", we compute an explicit correspondence between model and image edges. This allows us to treat the model edge vertices as a landmark with known 2D position, for which optimal pose or shape estimates can be easily computed.

[1] Matlab implementation: github.com/waps101/3DMM_edges

1.1. Preliminaries

Our approach is based on fitting a 3DMM to face images under the assumption of a scaled orthographic projection. Hence, we begin by describing the 3D morphable model and scaled orthographic projection.

Scaled orthographic projection The scaled orthographic, or weak perspective, projection model assumes that variation in depth over the object is small relative to the mean distance from camera to object. Under this assumption, the projected 2D position of a 3D point $\mathbf{v} = [u\ v\ w]^{\mathrm{T}}$ given by $\mathbf{SOP}[\mathbf{v}, \mathbf{R}, \mathbf{t}, s] \in \mathbb{R}^2$ does not depend on the distance of the point from the camera, but only on a uniform scale s given by the ratio of the focal length of the camera and the mean distance from camera to object:

$$\mathbf{SOP}[\mathbf{v}, \mathbf{R}, \mathbf{t}, s] = s \begin{bmatrix} 1 & 0 & 0 \\ 0 & 1 & 0 \end{bmatrix} \mathbf{R}\mathbf{v} + s\mathbf{t} \tag{1}$$

where the pose parameters $\mathbf{R} \in \mathbb{R}^{3\times3}$, $\mathbf{t} \in \mathbb{R}^2$ and $s \in \mathbb{R}^+$ are a rotation matrix, 2D translation and scale respectively.

3D Morphable Model A 3D morphable model is a deformable mesh whose shape is determined by the shape parameters $\boldsymbol{\alpha} \in \mathbb{R}^S$. Shape is described by a linear model learnt from data using Principal Components Analysis (PCA). So, the shape of any object from the same class as the training data can be approximated as:

$$\mathbf{s}(\boldsymbol{\alpha}) = \mathbf{P}\boldsymbol{\alpha} + \bar{\mathbf{s}}, \tag{2}$$

where $\mathbf{P} \in \mathbb{R}^{3N\times S}$ contains the S principal components, $\bar{\mathbf{s}} \in \mathbb{R}^{3N}$ is the mean shape and the vector $\mathbf{s}(\boldsymbol{\alpha}) \in \mathbb{R}^{3N}$ contains the coordinates of the N vertices, stacked to form a long vector: $\mathbf{s} = [u_1\ v_1\ w_1\ \ldots\ u_N\ v_N\ w_N]^{\mathrm{T}}$. Hence, the ith vertex is given by: $\mathbf{v}_i = [s_{3i-2}\ s_{3i-1}\ s_{3i}]^{\mathrm{T}}$.

For convenience, we denote the sub-matrix corresponding to the ith vertex as $\mathbf{P}_i \in \mathbb{R}^{3\times S}$ and the corresponding vertex in the mean face shape as $\bar{\mathbf{s}}_i \in \mathbb{R}^3$, such that the ith vertex is given by: $\mathbf{v}_i = \mathbf{P}_i\boldsymbol{\alpha} + \bar{\mathbf{s}}_i$. Similarly, we define the row corresponding to the u component of the ith vertex as $\mathbf{P}_{iu}$ (similarly for v and w) and define the u component of the ith mean shape vertex as $\bar{s}_{iu}$ (similarly for v and w).

2. FITTING WITH KNOWN CORRESPONDENCE

We begin by showing how to fit a morphable model to L observed 2D positions $\mathbf{x}_i = [x_i\ y_i]^{\mathrm{T}}$ $(i = 1 \ldots L)$ arising from the projection of corresponding vertices in the morphable model. We discuss in Section 3 how these correspondences are obtained in practice. Without loss of generality, we assume that the ith 2D position corresponds to the ith vertex in the morphable model. The objective of fitting a morphable model to these observations is to obtain the shape and pose parameters that minimise the reprojection error, E_{lmk}, between observed and predicted 2D positions:

$$E_{\text{lmk}} = \sum_{i=1}^{L} \| \mathbf{x}_i - \mathbf{SOP}\left[\mathbf{P}_i\boldsymbol{\alpha} + \bar{\mathbf{s}}_i, \mathbf{R}, \mathbf{t}, s\right] \|^2. \tag{3}$$

This problem is multilinear in the shape parameters and the SOP transformation matrix. It is also nonlinearly constrained, since $\mathbf{R}$ must be a valid rotation matrix. Although it is a non-convex optimisation problem, a good initialisation can be obtained using alternating linear least squares and this estimate subsequently refined using nonlinear optimisation.

Pose estimation We make an initial estimate of $\mathbf{R}$, $\mathbf{t}$ and s using a simple extension of the POS algorithm [17]. Compared to POS, we additionally enforce that $\mathbf{R}$ is a valid rotation matrix. We begin by solving an unconstrained system in a least squares sense. We stack two copies of the 3D points in homogeneous coordinates, such that $\mathbf{A}_{2i-1} = [u_i\ v_i\ w_i\ 1\ 0\ 0\ 0\ 0]$ and $\mathbf{A}_{2i} = [0\ 0\ 0\ 0\ u_i\ v_i\ w_i\ 1]$ and form a long vector of the corresponding 2D points $\mathbf{d} = [x_1\ y_1\ \cdots\ x_L\ y_L]^{\mathrm{T}}$. We then solve for $\mathbf{k} \in \mathbb{R}^8$ in $\mathbf{A}\mathbf{k} = \mathbf{d}$ using linear least squares. We define $\mathbf{r}_1 = [k_1\ k_2\ k_3]$ and $\mathbf{r}_2 = [k_5\ k_6\ k_7]$. Scale is given by $s = (\|\mathbf{r}_1\| + \|\mathbf{r}_2\|)/2$ and the translation vector by $\mathbf{t} = [k_4/s\ k_8/s]^{\mathrm{T}}$.

We perform singular value decomposition on the matrix formed from $\mathbf{r}_1$ and $\mathbf{r}_2$:

$$\mathbf{U}\mathbf{S}\mathbf{V}^{\mathrm{T}} = \begin{bmatrix} \mathbf{r}_1 \\ \mathbf{r}_2 \\ \mathbf{r}_1 \times \mathbf{r}_2 \end{bmatrix} \tag{4}$$

The rotation matrix is given by $\mathbf{R} = \mathbf{U}\mathbf{V}^{\mathrm{T}}$. If $\det(\mathbf{R}) = -1$ then we negate the third row of $\mathbf{U}$ and recompute $\mathbf{R}$. This guarantees that $\mathbf{R}$ is a valid rotation matrix. This approach gives a good initial estimate which we subsequently refine with nonlinear optimization.

Shape estimation With a fixed pose estimate, shape parameter estimation under scaled orthographic projection is a linear problem. The 2D position of the ith vertex as a function of the shape parameters is given by: $\mathbf{x}' = s\mathbf{R}_{1..2}(\mathbf{P}_i\mathbf{b} + \hat{\mathbf{s}}_i) + s\mathbf{t}$. Hence, each observed vertex adds two equations to a linear system. Concretely, for each image we form the matrix $\mathbf{C} \in \mathbb{R}^{2L\times S}$ where $\mathbf{C}_{2i-1} = s(\mathbf{R}_{11}\mathbf{P}_{iu}^{\mathrm{T}} + \mathbf{R}_{12}\mathbf{P}_{iv}^{\mathrm{T}} + \mathbf{R}_{13}\mathbf{P}_{iw}^{\mathrm{T}})$ and $\mathbf{C}_{2i} = s(\mathbf{R}_{21}\mathbf{P}_{iu}^{\mathrm{T}} + \mathbf{R}_{22}\mathbf{P}_{iv}^{\mathrm{T}} + \mathbf{R}_{23}\mathbf{P}_{iw}^{\mathrm{T}})$ and vector $\mathbf{h} \in \mathbb{R}^{2L}$ where $\mathbf{h}_{2i-1} = x_i - s(\mathbf{R}_1\hat{\mathbf{s}}_i + \mathbf{t}_1)$ and $\mathbf{h}_{2i} = y_i - s(\mathbf{R}_2\hat{\mathbf{s}}_i + \mathbf{t}_2)$. We solve $\mathbf{C}\mathbf{b} = \mathbf{h}$ in a least squares sense subject to an additional constraint to ensure plausibility of the solution. We follow Brunton et al. [18] and use a hyperbox constraint on the shape parameters. This ensures that each parameter lies within k standard deviations of the mean by introducing a linear inequality constraint on the shape parameters. We use a hard hyperbox constraint in preference to a soft elliptical prior as it avoids mean-shape bias and having to choose a regularisation weight.

Nonlinear refinement Finally, we perform nonlinear optimisation of E_{lmk} over $\boldsymbol{\alpha}$, $\mathbf{R}$, $\mathbf{t}$ and s simultaneously. We represent $\mathbf{R}$ in axis-angle space to ensure that it remains a valid rotation matrix and we retain the hyperbox constraint on $\boldsymbol{\alpha}$.

3. HARD EDGE CORRESPONDENCE

The fitting approach in Section 2 relies solely on geometric information, namely the 2D position of known vertices in the image. In practice, these positions and the correspondence to the model arises from two sources: landmarks and edges.

We initialise by applying a facial landmark detector that is suitable for operating on "in the wild" images. This provides approximate positions of facial landmarks for which we know the corresponding vertices in the morphable model. We use these landmark positions to make an initial estimate of the pose and shape parameters by running the method in Section 2 with only these corresponding landmark positions. Note that any facial landmark detector can be used at this stage. In our experiments, we show results with a recent landmark detection algorithm [19] that achieves state-of-the-art performance and for which code is provided by the authors.

From this initialisation, we proceed to fit to edges in an iterated closest point manner. That is, for each projected model contour vertex, we find the closest image edge pixel and we treat this as a new correspondence. In conjunction with the landmark correspondences, we again run the method in Section 2. This leads to updated pose and shape parameters, and in turn to updated model edges and correspondences. We iterate this process for K iterations. We illustrate the fitting procedure in Figure 1. On the left we show an input image with the initial landmark detection result. In the middle we show the initial shape and pose obtained by fitting only to landmarks. On the right we show image edge pixels in blue and projected model contours in green (where nearest neighbour edge correspondence is considered reliable) and in red (where correspondence is considered unreliable). The green/blue correspondences are used for the next iteration of fitting.

Model contours are computed based on the pose and shape parameters as the occluding boundary of the 3D face. Occluding boundary vertices are defined as those lying on an edge whose adjacent faces have a change of visibility. This definition encompasses both outer (silhouette) and inner (self-occluding) contours. Since the viewing direction is aligned with the z-axis, this is tested simply by checking if the sign of the z-component of the triangle normal changes on either side of the edge. In addition, we check that potential edge vertices are not occluded by another part of the mesh (using z-buffering) and we ignore edges that lie on the boundary of the mesh since they introduce artificial edges.

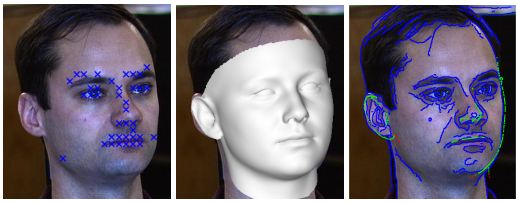

Fig. 1. Our edge fitting procedure (see text).

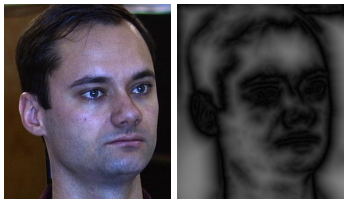

Fig. 2. Edge cost function (right) computed from input (left).

Finding the image edge pixel closest to a projected contour vertex can be done efficiently by storing the image edge pixels in a kd-tree. We filter the resulting correspondences using two commonly used heuristics. First, we remove 5% of the matches for which the distance to the closest image edge pixel is largest. Second, we remove matches for which the image distance divided by s exceeds a threshold (chosen as 10 in our experiments). The division by scale factor s makes this choice invariant to changes in image resolution.

In this paper, we deal only with occluding contours (both inner and outer). If texture contours were defined on the surface of the morphable model, it would be trivial to include these in our approach. Image edges are found by running the Canny edge detector with a fixed threshold.

4. SOFT EDGE CORRESPONDENCE

We compare our approach with a method based on optimising an edge cost function, in the same spirit as previous work [8, 9, 6]. We follow the same approach as Amberg et al. [8] to compute the edge cost function, however we further improve robustness by also integrating over scale. For our edge detector, we use gradient magnitude thresholding with non-maxima suppression. Given a set of edge detector sensitivity thresholds $\mathcal{T}$ and scales $\mathcal{S}$, we compute $n = |\mathcal{T} \times \mathcal{S}|$ edge images, $E^1, \ldots, E^n$, using each pair of image scale and threshold values. We compute the Euclidean distance transform, $D^1, \ldots, D^n$, for each edge image, before finally computing the edge cost function as:

$$E_{\text{edge}} = \frac{1}{n} \sum_{i=1}^{n} \frac{D^i}{D^i + \kappa}. \tag{5}$$

The parameter κ determines the influence range of an edge in an adaptive manner. Amberg et al. [8] suggest a value for κ of 1/20th the expected size of the head in pixels. We compute this parameter automatically from the scale s. An example of an edge cost surface is shown in Figure 2. To evaluate the edge cost, we compute model contour vertices as in Section 3, project them into the image and interpolate the edge cost function using bilinear interpolation.

For efficiency and to avoid problems of continuity and differentiability of the edge cost function, we follow [8] and keep occluding boundary vertices fixed for a number of iterations of the optimiser. After a number of iterations, we

Fig. 3. Synthetic input images for one subject.

	$-70°$	$-50°$	$-30°$	$-15°$	$0°$	$15°$	$30°$	$50°$	$70°$	Mean
Hard	2.77	2.64	2.77	2.74	2.64	2.71	2.65	2.68	2.77	2.71
Soft [6]	3.19	3.30	3.29	3.74	3.38	3.37	3.13	3.10	3.01	3.28

Table 1. Quantitative synthetic image results.

recompute the vertices lying on the occluding boundary and restart the optimiser. In practice, we found that optimising only the soft edge cost leads to highly unstable performance, even with the hyperbox constraint. So we also include a prior, $E_{\text{prior}} = \|\boldsymbol{\alpha}\|^2$. We minimise $E_{\text{lmk}} + w_1 E_{\text{edge}} + w_2 E_{\text{prior}}$ using the Levenberg-Marquardt algorithm. As for the hard correspondence method, we initialise by fitting to landmarks using the method in Section 2.

5. EXPERIMENTAL RESULTS

For the 3DMM in these experiments we use the Basel Face Model [20]. We begin with a quantitative comparative evaluation on synthetic data. We use the 10 out-of-sample faces supplied with the Basel Face Model and render orthographic images of each face in 9 poses (rotations of $0°$, $\pm 15°$, $\pm 30°$, $\pm 50°$ and $\pm 70°$ about the vertical axis). We show sample input images for one subject in Figure 3. We use the 70 Farkas landmarks, project the visible subset to the image (yielding between 37 and 65 landmarks per image) and round to the nearest pixel. These landmarks are used for initialisation. In Table 1 we report the mean Euclidean distance between ground truth and estimated face surface in mm after Procrustes alignment. We show results averaged over pose angle and over the whole dataset. Overall, our proposed approach achieves a $> 17\%$ reduction in error over the soft correspondence approach [6]. Moreover, our method is an order of magnitude faster (average running time 13s versus 157s).

Next in Figure 4 we show qualitative examples from the CMU PIE [21] dataset. Here, we fit to images in a non-frontal pose using automatically detected landmarks [19], texture map the image onto the mesh, rotate to frontal pose and compare to an actual frontal view. Finally, we show qualitative examples from the Labelled Faces in the Wild dataset [22] in Figure 5. Again, we texture map the image to the mesh and show a range of poses. These results show that our method is capable of robustly and fully automatically fitting to unconstrained images.

6. CONCLUSIONS

We have presented a fully automatic algorithm for fitting a 3DMM to single images using hard edge correspondence and

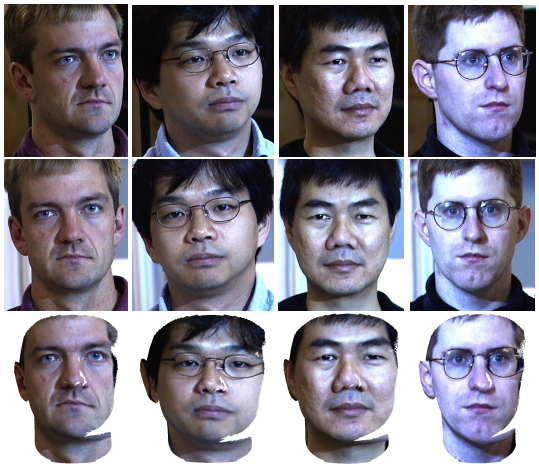

Fig. 4. Qualitative frontalisation results.

Fig. 5. Qualitative pose editing results.

compared it to existing methods using soft correspondence. In 3D-3D alignment, the soft correspondence of LM-ICP [7] is demonstrably more robust than hard ICP [16]. However, in the context of 3D-2D nonrigid alignment, a soft edge cost function is neither continuous nor differentiable since contours appear, disappear, split and merge under parameter changes [9]. This makes its optimisation challenging, unstable and highly dependent on careful choice of optimisation parameters. Although our proposed algorithm relies on potentially brittle hard correspondences, solving for shape and pose separately requires only solution of a linear problem and, together, optimisation of a multilinear problem. This makes it very fast and seemingly less sensitive to local minima. We envisage that our method will provide a baseline or fast initialisation that other methods can build upon.

There are many ways this work can be extended. First, we could explore other ways in which the notion of soft correspondence is formulated. For example, we could borrow from SoftPOSIT [23] or Blind PnP [24] which both estimate pose with unknown 3D-2D correspondence. Second, we could incorporate any of the refinements to standard ICP [25]. Third, we currently use only geometric information and do not fit texture. Finally, we would like to extend the method to video using a model that captures expression variation and incorporating temporal smoothness constraints.

7. REFERENCES

[1] T. F. Cootes, C. J. Taylor, D. Cooper, and J. Graham, "Active shape models – their training and application," *Comput. Vis. Image Underst.*, vol. 61, pp. 38–59, 1995.

[2] G. A. Atkinson, M. L. Smith, L. N. Smith, and A. R. Farooq, "Facial geometry estimation using photometric stereo and profile views," in *Proc. International Conference on Biometrics*, 2009.

[3] V. Blanz and T. Vetter, "A morphable model for the synthesis of 3D faces," in *SIGGRAPH*, 1999.

[4] B. Moghaddam, J. Lee, H. Pfister, and R. Machiraju, "Model-based 3d face capture with shape-from-silhouettes," in *FG*, 2003.

[5] M. Lüthi, T. Albrecht, and T. Vetter, "Probabilistic modeling and visualization of the flexibility in morphable models," in *Math. of Surf. XIII*, 2009.

[6] S. Romdhani and T. Vetter, "Estimating 3D shape and texture using pixel intensity, edges, specular highlights, texture constraints and a prior," in *CVPR*, 2005.

[7] A. W. Fitzgibbon, "Robust registration of 2d and 3d point sets," *Image Vis. Comput.*, vol. 21, no. 13, pp. 1145–1153, 2003.

[8] B. Amberg, A. Blake, A. Fitzgibbon, S. Romdhani, and T. Vetter, "Reconstructing high quality face-surfaces using model based stereo," in *ICCV*, 2007.

[9] M. Keller, R. Knothe, and T. Vetter, "3D reconstruction of human faces from occluding contours," in *MIRAGE*, 2007.

[10] D. Sánchez-Escobedo, M. Castelán, and W.A.P. Smith, "Statistical 3D face shape estimation from occluding contours," *Comput. Vis. Image Underst.*, vol. 142, no. 111-124, 2016.

[11] P. Breuer, K. Kim, W. Kienzle, B. Schölkopf, and V. Blanz, "Automatic 3D face reconstruction from single images or video," in *Proc. FG*, 2008, pp. 1–8.

[12] O. Aldrian and W. A. P. Smith, "Inverse rendering of faces with a 3D morphable model," *IEEE Trans. Pattern Anal. Mach. Intell.*, vol. 35, no. 5, pp. 1080–1093, 2013.

[13] B. Amberg and T. Vetter, "Optimal landmark detection using shape models and branch and bound," in *Proc. ICCV*, 2011.

[14] S. Schönborn, A. Forster, B. Egger, and T. Vetter, "A monte carlo strategy to integrate detection and model-based face analysis," *Patt. Rec.*, pp. 101–110, 2013.

[15] P. Huber, Z. Feng, W. Christmas, J. Kittler, and M. Rätsch, "Fitting 3D morphable models using local features," in *ICIP*, 2015.

[16] P. J. Besl and N. D. McKay, "A method for registration of 3-D shapes," *IEEE Trans. Pattern Anal. Mach. Intell.*, vol. 14, no. 2, pp. 239—256, 1992.

[17] D. F. Dementhon and L. S. Davis, "Model-based object pose in 25 lines of code," *Int. J. Comput. Vis.*, vol. 15, no. 1-2, pp. 123–141, 1995.

[18] A. Brunton, A. Salazar, T. Bolkart, and S. Wuhrer, "Review of statistical shape spaces for 3D data with comparative analysis for human faces," *Comput. Vis. Image Underst.*, vol. 128, pp. 1–17, 2014.

[19] X. Zhu and D. Ramanan, "Face detection, pose estimation, and landmark localization in the wild," in *Proc. CVPR*, 2012.

[20] P. Paysan, R. Knothe, B. Amberg, S. Romdhani, and T. Vetter, "A 3D face model for pose and illumination invariant face recognition," in *Proc. IEEE Intl. Conf. on Advanced Video and Signal based Surveillance*, 2009.

[21] T. Sim, S. Baker, and M. Bsat, "The CMU pose, illumination, and expression database," *IEEE Trans. Pattern Anal. Mach. Intell.*, vol. 25, no. 12, pp. 1615–1618, 2003.

[22] Gary B. Huang, Manu Ramesh, Tamara Berg, and Erik Learned-Miller, "Labeled faces in the wild: A database for studying face recognition in unconstrained environments," Tech. Rep. 07-49, University of Massachusetts, Amherst, October 2007.

[23] P. David, D. DeMenthon, R. Duraiswami, and H. Samet, "SoftPOSIT: Simultaneous pose and correspondence determination," in *Proc. ECCV*, 2002, pp. 698–714.

[24] F. Moreno-Noguer, V. Lepetit, and P. Fua, "Pose priors for simultaneously solving alignment and correspondence," in *Proc. ECCV*, 2008, pp. 405–418.

[25] S. Rusinkiewicz and M. Levoy, "Efficient variants of the icp algorithm," in *Proc. 3DIM*, 2001.